

Gas Transport Mechanisms through Molecular Thin Carbon Nanomembranes

Vladislav Stroganov, Daniel Hüger, Christof Neumann, Tabata Noethel, Michael Steinert, Uwe Hübner, and Andrey Turchanin*

Molecular thin carbon nanomembranes (CNMs) synthesized by electron irradiation induced cross-linking of aromatic self-assembled monolayers (SAMs) are promising 2D materials for the next generation of filtration technologies. Their unique properties including ultimately low thickness of ≈ 1 nm, sub-nanometer porosity, mechanical and chemical stability are attractive for the development of innovative filters with low energy consumption, improved selectivity, and robustness. However, the permeation mechanisms through CNMs resulting in, e.g., an ≈ 1000 times higher fluxes of water in comparison to helium have not been yet understood. Here, a study of the permeation of He, Ne, D₂, CO₂, Ar, O₂ and D₂O using mass spectrometry in the temperature range from room temperature to ≈ 120 °C is studied. As a model system, CNMs made from [1'',4',1',1]-terphenyl-4-thiol SAMs are investigated. It is found out that all studied gases experience an activation energy barrier upon the permeation which scales with their kinetic diameters. Moreover, their permeation rates are dependent on the adsorption on the nanomembrane surface. These findings enable to rationalize the permeation mechanisms and establish a model, which paves the way toward the rational design not only of CNMs but also of other organic and inorganic 2D materials for energy-efficient and highly selective filtration applications.


1. Introduction

In order to reduce the energy consumption in filtration technologies, there is a high and continuous demand for new

V. Stroganov, D. Hüger, C. Neumann, T. Noethel, A. Turchanin
Institute of Physical Chemistry
Friedrich Schiller University Jena
07743 Jena, Germany
E-mail: andrey.turchanin@uni-jena.de

M. Steinert
Institute of Applied Physics
Friedrich Schiller University Jena
07743 Jena, Germany

U. Hübner
Leibniz Institute of Photonic Technology (IPHT)
07745 Jena, Germany

 The ORCID identification number(s) for the author(s) of this article can be found under <https://doi.org/10.1002/sml.202300282>.

© 2023 The Authors. Small published by Wiley-VCH GmbH. This is an open access article under the terms of the Creative Commons Attribution-NonCommercial-NoDerivs License, which permits use and distribution in any medium, provided the original work is properly cited, the use is non-commercial and no modifications or adaptations are made.

DOI: 10.1002/sml.202300282

membrane materials.^[1] In this respect 2D materials such as ≈ 1 nm thick carbon nanomembranes (CNMs) possess a great promise.^[2] CNMs can be synthesized on large scale by electron-irradiation induced cross-linking of aromatic self-assembled monolayers^[3] and combine a number of unique properties including extremely low ≈ 1 nm thickness,^[2] sub-nanometer porosity,^[4] high mechanical^[5] and chemical stability.^[2] These properties enable to engineer energy-efficient nanomembranes for filtration which can operate at low-pressure differences and simultaneously maintain high fluxes of the permeates.^[4,6] However, the permeation mechanisms through CNMs remain largely unknown.^[7] In particular, it concerns the ≈ 1000 times higher permeation of water in comparison to helium as well as its non-linear dependence on the partial vapor pressure.^[4] A nonlinear permeation behavior of water was also reported for thick polymer-based membranes^[8] and described by the solution-diffusion model.^[9] In this model, the

gases dissolve in a membrane and diffuse across it driven by a difference in the chemical potentials. As dissolution of water in the 2D membranes is hardly possible due to their extremely low thickness, most probably the adsorption-diffusion mechanism^[10] governs the permeation. In this case, the permeant species initially adsorb on the nanomembrane surface and then diffuse across it overcoming a certain activation energy barrier. Therewith, the permeation depends on two material parameters: i) Enthalpy of adsorption (ΔH_{ads}) and ii) activation energy of diffusion (E_{diff}). To reveal the permeation mechanism through CNMs, we conducted a permeation study of He, Ne, D₂, CO₂, Ar, O₂ and D₂O in the temperature range from room temperature (RT) to ≈ 120 °C employing an experimental setup based on mass spectrometry. This selection of gases enables us to vary the kinetic diameter of the permeates as well as their enthalpy of adsorption. As a model system, we investigated CNMs made from [1'',4',1',1]-terphenyl-4-thiols (TPT CNMs). Our systemic study clearly reveals the adsorption-diffusion mechanism of the gas permeation through ≈ 1 nm thick TPT CNMs and explains the permeation results observed in CNMs including the ≈ 1000 higher permeation rate of water in comparison to helium. These findings pave the way to the rational design of the energy efficient molecular nanomembranes for a variety of filtration and gas separation applications.

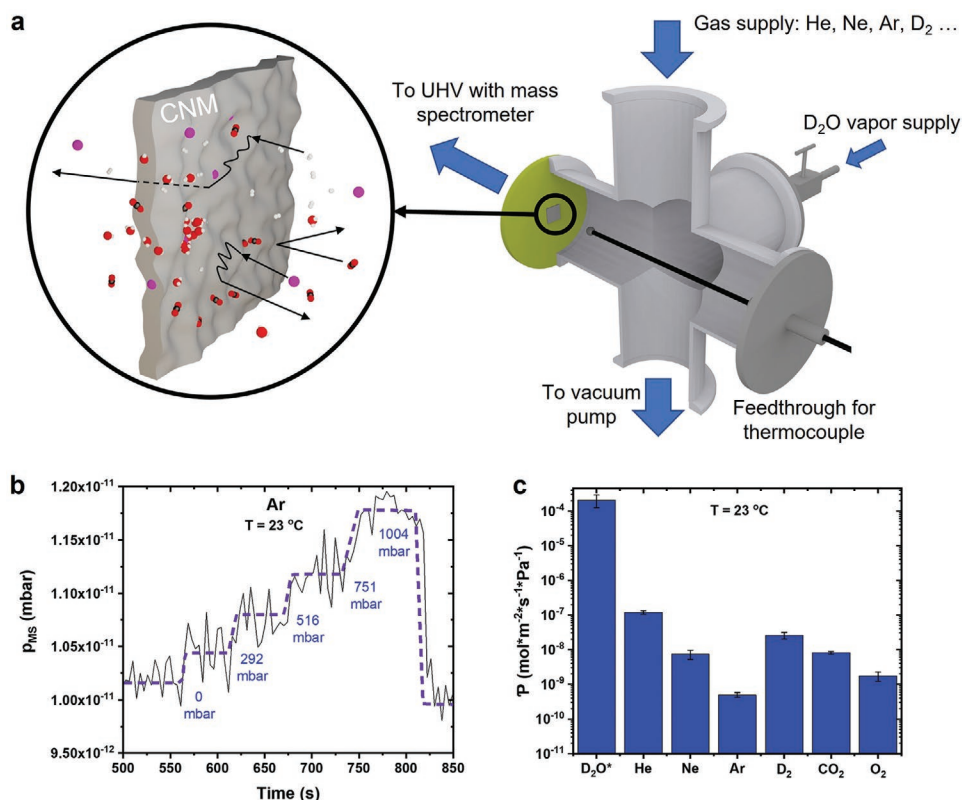


Figure 1. Permeation of various gases through carbon nanomembrane (CNM) at RT. a) Left part schematically represents different events happening upon the permeation through CNMs. Black arrows and lines demonstrate possible paths of the gas molecules caused by adsorption–diffusion, adsorption–desorption, or deflection. Right part schematically represents the experimental setup used for the permeation measurements (see Section S3, Supporting Information for details). Sample holder with a CNM is fixed between the gas chamber and the UHV MS chamber. Temperature of the gas chamber and the sample can be tuned by heating. b) Pressure as detected by MS (p_{MS}) for different applied p_{Ar} at RT (23 °C). The dashed line is a guide to the eye. c) Summary of the RT permeances for TPT CNM. An average value is taken for three different samples, error bars represent the standard deviation. Noble and multiatomic gases are grouped to emphasize the correlation between their permeances and molecular kinetic diameters. *D₂O is an exception from this trend, as its permeance depends on the partial vapor pressure; the value presented here is calculated at $p_{D_2O} = 24$ mbar, which is close to the saturated vapor pressure.

2. Results and Discussion

2.1. Permeation of Gases at Room Temperature

Measurements of the gas permeation through CNMs were performed using a sensitive mass spectrometer (MS) operating in an ultra-high vacuum (UHV) chamber. The experimental setup is schematically presented in Figure 1a (for details see Section S1 and Figure S1, Supporting Information). The CNM acts here as a membrane separating the chamber with the gases and the vacuum chamber with the MS. Therefore, the gas molecules can be detected by the MS only if they permeate through the CNM. In Figure 1b the MS signal obtained for Ar at room temperature (RT) and different applied pressures is shown. Despite the low signal-to-noise ratio a clear linear correlation of the signal with increasing pressure is observed, which enables to calculate the permeance, \mathcal{P} (see Section S2, Supporting Information). Measurements of other gases—He, Ne, D₂, CO₂, O₂ and D₂O—revealed higher values of the respective MS signals. Note that in our study we use D₂ instead of H₂, and D₂O instead of H₂O due to high background levels of the respective

MS signals at masses 2 and 18. Background levels at masses 4 and 20 are low enough to enable the reliable MS detection of D₂ and D₂O. A summary of the obtained permeances for all studied gases is presented in Figure 1c. As can be seen, the permeance of D₂O is ≈ 1000 times higher than the permeance of He and other gases. This result for He and D₂O is consistent with the previous study.^[4] However, in this study, only the permeation of He and H₂O which have small kinetic diameters was reported, whereas we observe the permeation also of the bigger gases. We attribute this difference to the improved sensitivity in our experiments. It is also notable that the permeance of noble gases decreases with increasing atomic number and a decrease of the permeance is observed for multiatomic gases in the sequence D₂, CO₂, O₂. These dependencies can be attributed either to the lower impingement rates for heavier gases or to the presence of energy barrier of the permeation, which is dependent on the permeating species. As the impingement rate is inversely proportional to the square root of the molecular masses, its effect is too small to explain the several orders of magnitude variation of the permeances for He, Ne, D₂, CO₂, O₂ and D₂O.

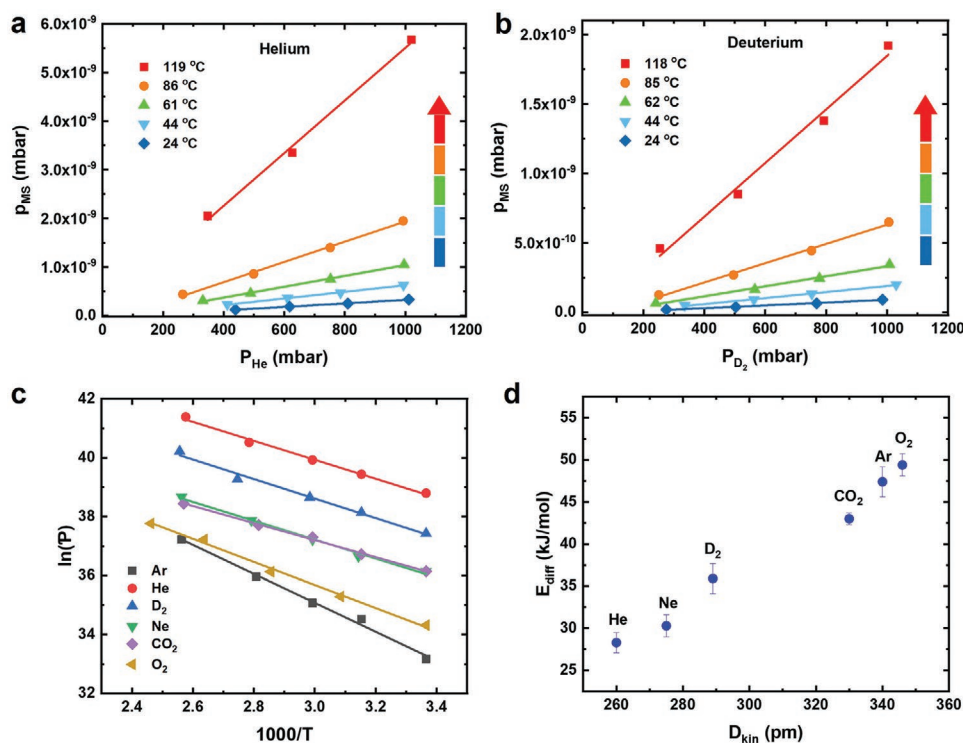


Figure 2. Temperature-dependent permeation of different gases. a,b) Dependencies of the mass spectrometer signal for He and D₂, respectively, as functions of their partial pressures and temperature. c) Arrhenius plots of the permeances of the studied gases. The lines in a, b and c are linear fits. d) The plot shows a correlation between the activation energy of diffusion and kinetic diameters of different gases.

2.2. Permeation of Gases at Elevated Temperatures

To study the assumed activation energy related mechanisms of the permeation through CNMs, we proceed with the measurements at variable temperature. **Figure 2a,b** shows examples of the respective He and D₂ signals in the temperature range from RT to ≈120 °C. The signals of mass spectrometer increase with increasing temperature with the slopes proportional to the respective permeances. We calculate that the permeance of He increases from $1.36 \times 10^{-7} \text{ mol m}^{-2} \text{ s}^{-1} \text{ Pa}^{-1}$ at RT to $1.76 \times 10^{-6} \text{ mol m}^{-2} \text{ s}^{-1} \text{ Pa}^{-1}$ at 119 °C. The character of this increase provides information on the permeation mechanisms. One possibility is that the Knudsen effusion is the dominant permeation mechanism for weakly adsorbing gases, as was reported for thin (200–500 nm) polymer membranes.^[11] This mechanism is applicable for membranes with effective pore diameters bigger than the permeating gas molecules under the free molecular flow regime.^[12] However, the studied CNM samples do not have any microscopic pores as studied by SEM (Section S3 and Figure S4, Supporting Information) as well as the earlier studies report only subnanometer porosity in this material.^[4,13] Additionally, Knudsen effusion coefficient is proportional to a square root of temperature, i.e., to \sqrt{T} .^[14] This weak temperature dependence cannot explain an increase of the helium permeance by one order of magnitude in the studied temperature range of about 100 K. Therefore, we conclude that Knudsen effusion is unlikely to be the dominant transport mechanism through the CNMs for weakly adsorbing gases.

Another possible explanation of the increase of the permeation with increasing temperature is the presence of an energy barrier with the permeance following the Arrhenius behavior.^[15] To prove this hypothesis, we plot the obtained permeances in the Arrhenius coordinates and obtain linear dependencies, Figure 2c. The slope of each line corresponds to $-\frac{E_a}{R}$, where E_a is the apparent activation energy of permeation and R is the universal gas constant. The obtained values of E_a for each gas are presented in Table S1 (Supporting Information). As can be seen, these data do not correlate with the kinetic diameters of the studied gases. To rationalize this discrepancy, we apply a two-step model to describe the permeation behavior, which can be presented as



The first step represents an equilibrium for the species M between the gas phase and the adsorbates on the CNM surface. The second step represents diffusion of these species through the CNM. In total, the permeation mechanism includes two energy contributions: enthalpy of adsorption, ΔH_{ads} , and activation energy of diffusion, E_{diff} . Therewith, the total apparent activation energy, E_a , of the permeation is given as $E_a = E_{\text{diff}} + \Delta H_{\text{ads}}$. Quantitatively the permeation through a 2D membrane can be described by

$$P = P_0 \times \exp\left(-\frac{\Delta S}{R}\right) \times \exp\left(-\frac{E_{\text{diff}} + \Delta H_{\text{ads}}}{RT}\right) \quad (2)$$

where \mathcal{P} is the permeance, \mathcal{P}_0 is the exponential pre-factor, ΔS is the entropy change upon the permeation, R is the universal gas constant and T is the absolute temperature.^[10a] By using Equation (2) and knowing of the ΔH_{ads} data for the CNM, the E_{diff} data can be calculated. As the ΔH_{ads} data for CNMs have not been determined yet, we apply the adsorption enthalpies of the studied gases reported for related carbon-based materials (see Section S4 and Table S1, Supporting Information). Figure 2d summarizes the obtained E_{diff} data plotted as a function of the kinetic diameters. For all studied gases the E_{diff} values correlate with their kinetic diameters—the bigger gases experience the higher activation barriers. This finding clearly supports the adsorption-diffusion permeation mechanism through the CNM. It further agrees with the suggested subnanometer porosity^[4,13] for the studied TPT CNMs which excludes the ballistic transport of gases across these nanomembranes. Furthermore, the linear dependence of the permeation for the weakly adsorbing gases as a function of their partial pressures (see Figure 2a,b) can now be well rationalized by the Henry-type (linear) adsorption isotherms for these species on the CNM surface.^[16]

2.3. Temperature-Dependent Permeation of Water

In contrast to other gases, D_2O shows a nonlinear permeation behavior as a function of the partial pressure for all studied temperatures (Figure 3a). Moreover, in contrast to He, Ne, D_2 , CO_2 , Ar, O_2 the permeation decreases with increasing temperature. These functional dependencies resemble the shape of Brunauer-Emmett-Teller (BET) adsorption isotherms for adsorption of multilayers in which there is a higher affinity between adsorbate species than between adsorbate and substrate.^[17] We suggest that this observation is not a coincidence but rather a reflection of the adsorption behavior of D_2O on the CNM surface; similarly, as the observed Henry-type adsorption, e.g., for He described in the previous paragraph. Next, in order to rationalize an ≈ 1000 times higher permeation of D_2O in comparison to He we refer now to Equation (2). As can be seen, the permeance increases exponentially with decreasing entropy during the permeation. Therewith, it is straightforward that for weakly interacting species, like, e.g., He, a decrease of the entropy is lower than for species having a higher affinity to each other,

like D_2O , and therefore a higher permeance can be expected for the latter. Moreover, if multilayers of D_2O are formed, the transformation to a nearly condensed, liquid-like phase will further decrease the entropy and enhance the permeation. As reported earlier for TPT CNMs,^[4] the permeation of water at a vapor pressure close to the saturation has a similar value as for liquid water. This result suggests that water (or in our case D_2O) condenses on the CNM surface^[7] leading to a significantly increased permeation. Equation (2) can be applied to give a quantitative explanation to this phenomenon. We estimate a difference of the permeances of H_2O (D_2O) versus CO_2 due to the entropy change (Section S5, Supporting Information) using the data reported for zeolites.^[18] The result predicts a factor of 2.5×10^4 higher permeance of H_2O (D_2O), which is close to the values presented in Figure 1c.

In the following, we discuss a decrease of the permeation of D_2O with increasing temperature. This behavior corresponds to negative values of the apparent activation energy meaning that $|E_{\text{diff}}| < |\Delta H_{\text{ads}}|$ (see Equation (2)). As the kinetic diameter of D_2O (265 pm) is close to that of He (260 pm),^[19] we can assume for D_2O nearly the same E_{diff} value as experimentally obtained for He (see Figure 2d).

The reported values of ΔH_{ads} for water on carbon materials are in the range from -45 to -69 kJ mol^{-1} .^[20] These values result in the negative E_a and therefore in decrease of the permeation with increasing temperature, as observed in our experiment. Note that negative apparent activation energy in chemical kinetics is a signature of processes with pre-equilibria. In case of the water permeation through CNMs the adsorption on their surface and the subsequent diffusion across the membrane (see Equation 1).

In Figure 3b, the Arrhenius plots of the D_2O permeance are presented as functions of the partial pressure. One can clearly recognize their non-linear behavior. Interestingly, similar dependencies were reported for thick polymeric membranes if the permeation was studied at temperatures below the critical temperatures of the permeating gases.^[8,21] In this case both E_a and ΔS are dependent on pressure and temperature. Based on the data presented in Figure 3b we estimate a range of E_a from -10 to -40 kJ mol^{-1} . With these data and the value of $E_{\text{diff}} \approx 29$ kJ mol^{-1} , we calculate the respective ΔH_{ads} values to be in the range from -39 to -69 kJ mol^{-1} . These values correspond

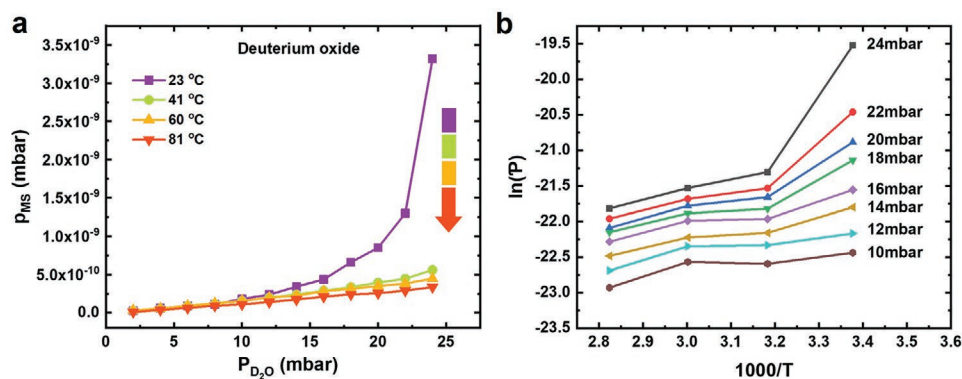


Figure 3. Temperature-dependent permeation of D_2O vapor. a) Influence of the feed pressure of D_2O vapor on signal of the mass spectrometer at different temperatures. b) The Arrhenius plot of permeance of D_2O against temperature at different feed pressures. The lines in a and b are to guide the eye.

well to the experimental data (see previous paragraph), which further validates the suggested permeation model.

2.4. Selectivity of Permeation

Commercial filtration and separation processes are often performed at temperatures where the balance between selectivity, permeability, and costs of operation is reached. Thus, it is important to consider selectivity of separation of different gas pairs at different temperatures. In general, the selectivity of permeation of different gas pairs is the result of their different permeabilities, which in turn are defined by the diffusion and adsorption coefficients. The diffusion coefficient depends on the size of the penetrant and the molecular structure of the membrane matrix. The adsorption coefficient is determined by the chemical nature of the penetrant and the surface of the membrane. The interplay of these parameters defines the final selectivity ratios. For example, the recent reports showed dramatically increased selectivity of CO₂ permeation relative to other gases on the novel polymer membranes with increased affinity toward CO₂.^[22] In **Figure 4**, we summarized the selectivity data for different industrially important gas pairs. One of the most notable pairs is D₂O/D₂ with the selectivity of ≈3000 at RT, which is explained by the higher adsorption of D₂O on the surface of the CNM than of D₂. This value however is calculated for the saturated D₂O vapor pressure of ≈24 mbar, which cannot be higher at this temperature. Usually, water/hydrogen separation is conducted at elevated temperatures. Our experiments show that selectivity of the separation of D₂O/D₂ at 120 °C is ≈50, which demonstrates that TPT CNM can be a candidate for hydrogen drying upon the water electrolysis processes.

3. Conclusions

In summary, based on a systematic study of the temperature-dependent permeation for a selection of gases with variable

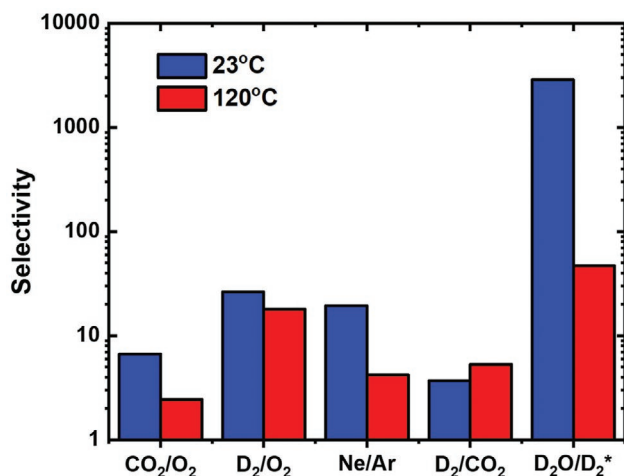


Figure 4. Separation selectivity. Selectivities of different gas pairs at room temperature and 120 °C. *The selectivity of the D₂O/D₂ pair was calculated for 24 mbar of D₂O vapor pressure.

kinetic diameters and the chemical affinity we reveal the permeation mechanism through ultrathin (≈1 nm) molecular nanomembranes with sub-nanometer porosity. The permeation process consists of two steps: i) Adsorption of the permeant on the nanomembrane surface and ii) its diffusion across the nanomembrane. These steps are characterized by the respective enthalpy of adsorption, ΔH_{ads} , and the activation energy of diffusion, E_{diff} . A combination of both these quantities defines the final apparent activation energy of the permeation, E_a , and the respective permeation rates. These findings enable to rationalize an increase of the permeation with increasing temperature for such gases like He, Ne, D₂, CO₂, Ar, O₂ and its decrease for D₂O, as well the non-linear behavior of the permeation D₂O (H₂O) as a function of the partial pressure. Moreover, the entropy changes upon the permeation of D₂O versus He elucidates a ≈1000 times higher permeation rate of D₂O despite the similar kinetic diameters of these gases. The current work has demonstrated that the permeation of gases through ultrathin 2D materials is governed by the fundamental adsorption-diffusion mechanism which is applicable for a wide range of gases and vapors. The obtained mechanistic details of the permeation through nanoporous ultrathin molecular nanomembranes facilitate engineering of the tailored nanomembranes from 2D materials for energy efficient gas filtration and separation technologies.

4. Experimental Section

Preparation of Freestanding CNMs: To synthesize CNMs, the self-assembled monolayers (SAMs) of [1'',4',1',1]-terphenyl-4-thiol (TPT) (Sigma Aldrich, 97%) were prepared on 300 nm thick Au layers on mica substrates (Georg Albert PVD-Coatings). To this end, the Au substrates were cleaned with oxygen plasma and immersed in a dry and degassed solution of TPT in dimethylformamide (DMF) for 24 h at 70 °C for SAM formation. After the self-assembly, samples were washed with DMF and ethanol and dried under nitrogen flow. The cross-linking of SAMs into CNMs was subsequently conducted in high vacuum ($<5 \times 10^{-8}$ mbar) by irradiation with an electron gun (FG15/40 Specs) using an electron energy of 50 eV and an electron dose of 50 mC cm⁻².

Transfer of the CNMs was performed using a stabilizing ≈1 μm thick polymethylmethacrylate (PMMA) layer which was spin-coated onto the CNM surface. The PMMA/CNM/Au film was mechanically detached from mica and transferred onto a I₂/KI bath to dissolve gold. Afterward the PMMA/CNM film was placed onto a NaS₂O₃ bath to remove iodine residues. The film was then washed in a water bath twice to remove traces of salts and then transferred to the target Si₃N₄ substrate with a circular opening 5.1 μm in diameter for the permeation studies (see Section S6 and Figure S5, Supporting Information). The PMMA layer was dissolved by immersing the sample in acetone, and supercritical CO₂ drying was applied to remove the sample from liquid without destroying the free-standing CNM area by surface tension.^[23] Finally, before the permeation studies, the samples were controlled for the absence of defects like ruptures and pinholes by a procedure described in Sections S1 and S2 and Figure S2 (Supporting Information).

Mass Spectrometry Measurements of the Permeances: Mass spectrometry measurements were employed to study the permeances of gaseous He, Ne, D₂, CO₂, Ar, O₂ and D₂O through the CNMs using a mass spectrometer (Hiden Analytical HAL3F-RC) installed in an ultra-high vacuum (UHV) chamber with the base pressure of ≈6 × 10⁻¹⁰ mbar. He (Linde, 99.996%) Ne, D₂, CO₂, Ar, O₂ (Linde, 99.999%), D₂ (Linde, 99.8%) and D₂O (Acros Organics, 99.8 at.%) purity were used in the experiments. The scheme of the experimental setup and

the measurement procedures are described in Section S1 and Figure S1 (Supporting Information). Calibration of the setup, evaluation of the results and calculations of the permeances are presented in detail in Section S2 and Figures S2 and S3 (Supporting Information).

Microscopy: The optical microscopy of supported and suspended CNMs was conducted in the bright-field mode using a Zeiss Axio Imager Z1.m microscope equipped with a 5-megapixel CCD camera (AxioCam ICc5) before and after the permeation measurements. Besides that, selected samples were characterized, after completing the permeation studies, via scanning electron microscopy (SEM) with a Sigma VP microscope (Carl Zeiss) at a beam energy of 15 kV using the in-lens detector. Note that SEM imaging can influence the structure of CNMs and therewith modify their permeation characteristics; therefore, samples characterized by SEM were not used for further permeation studies.

Supporting Information

Supporting Information is available from the Wiley Online Library or from the author.

Acknowledgements

The authors thank Deutsche Forschungsgemeinschaft DFG for funding via the Transregio-Collaborative Research Center TRR234 “Catalight” (Project B7). The authors acknowledge Stephanie Höppener and Ulrich S. Schubert for providing access to the scanning electron microscope. The SEM facilities of the Jena Center for Soft Matter (JCSM) were established with a grant from the DFG.

Open access funding enabled and organized by Projekt DEAL.

Conflict of Interest

The authors declare no conflict of interest.

Data Availability Statement

The data that support the findings of this study are available from the corresponding author upon reasonable request.

Keywords

2D materials, carbon nanomembranes, permeation mechanisms, separation technologies, nanofiltration

Received: January 10, 2023

Revised: March 4, 2023

Published online: April 7, 2023

- [1] a) A. Alabi, A. AlHajaj, L. Cseri, G. Szekely, P. Budd, L. Zou, *npj Clean Water* **2018**, 1, 10; b) Z. Yang, P.-F. Sun, X. Li, B. Gan, L. Wang,

- X. Song, H.-D. Park, C. Y. Tang, *Environ. Sci. Technol.* **2020**, 54, 15563.
[2] A. Turchanin, A. Gözlhäuser, *Adv. Mater.* **2016**, 28, 6075.
[3] P. Angelova, H. Vieker, N.-E. Weber, D. Matei, O. Reimer, I. Meier, S. Kurasch, J. Biskupek, D. Lorbach, K. Wunderlich, L. Chen, A. Terfort, M. Klapper, K. Müllen, U. Kaiser, A. Gözlhäuser, A. Turchanin, *ACS Nano* **2013**, 7, 6489.
[4] Y. Yang, P. Dementyev, N. Biere, D. Emmrich, P. Stohmann, R. Korzetz, X. Zhang, A. Beyer, S. Koch, D. Anselmetti, A. Gözlhäuser, *ACS Nano* **2018**, 12, 4695.
[5] X. Zhang, A. Beyer, *Nanoscale* **2021**, 13, 1443.
[6] a) M. Ai, S. Shishatskiy, J. Wind, X. Zhang, C. T. Nottbohm, N. Mellech, A. Winter, H. Vieker, J. Qiu, K.-J. Dietz, A. Gözlhäuser, A. Beyer, *Adv. Mater.* **2014**, 26, 3421; b) P. M. G. van Deursen, Z. Tang, A. Winter, M. J. Mohn, U. Kaiser, A. A. Turchanin, G. F. Schneider, *Nanoscale* **2019**, 11, 20785; c) Y. Yang, R. Hillmann, Y. Qi, R. Korzetz, N. Biere, D. Emmrich, M. Westphal, B. Büker, A. Hütten, A. Beyer, D. Anselmetti, A. Gözlhäuser, *Adv. Mater.* **2020**, 32, 1907850.
[7] P. Dementyev, T. Wilke, D. Naberezhnyi, D. Emmrich, A. Gözlhäuser, *Phys. Chem. Chem. Phys.* **2019**, 21, 15471.
[8] a) S. Stern, S. Fang, R. Jobbins, *J. Metabolomics Syst. Biol.* **1971**, 5, 41; b) S. A. Stern, J. T. Mullhaupt, P. J. Gareis, *Open Med. Chem. J.* **1969**, 15, 64.
[9] J. G. Wijmans, R. W. Baker, *J. Membr. Sci.* **1995**, 107, 1.
[10] a) P. Z. Sun, M. Yagmurcukardes, R. Zhang, W. J. Kuang, M. Lozada-Hidalgo, B. L. Liu, H. M. Cheng, F. C. Wang, F. M. Peeters, I. V. Grigorieva, A. K. Geim, *Nat. Commun.* **2021**, 12, 7170; b) S. P. Koenig, L. Wang, J. Pellegrino, J. S. Bunch, *Nat. Nanotechnol.* **2012**, 7, 728.
[11] G. Firpo, E. Angeli, L. Repetto, U. Valbusa, *J. Membr. Sci.* **2015**, 481, 1.
[12] K. Malek, M.-O. Coppens, *J. Chem. Phys.* **2003**, 119, 2801.
[13] P. Dementyev, Y. Yang, M. Rezvova, A. Gözlhäuser, *J. Phys. Chem. Lett.* **2020**, 11, 238.
[14] J. Welty, C. E. Wicks, G. L. Rorrer, R. E. Wilson, *Fundamentals of Momentum, Heat and Mass Transfer*, Wiley, New York **2007**.
[15] K. A. Stevens, J. D. Moon, H. Borjigin, R. Liu, R. M. Joseph, J. S. Riffle, B. D. Freeman, *J. Membr. Sci.* **2020**, 593, 117427.
[16] H. Y. Erbil, *Surface Chemistry of Solid and Liquid Interfaces*, Wiley, New York **2006**.
[17] a) S. Brunauer, L. S. Deming, W. E. Deming, E. Teller, *J. Am. Chem. Soc.* **1940**, 62, 1723; b) S. Brunauer, P. H. Emmett, E. Teller, *J. Am. Chem. Soc.* **1938**, 60, 309.
[18] A. Budi, S. L. S. Stipp, M. P. Andersson, *J. Phys. Chem. C* **2018**, 122, 8236.
[19] A. F. Ismail, K. C. Khulbe, T. Matsuura, *Gas Separation Membranes: Polymeric and Inorganic*, Springer International Publishing, New York **2015**.
[20] a) S. Qi, K. J. Hay, M. J. Rood, M. P. Cal, *J. Environ. Eng.* **2000**, 126, 267; b) S. W. Rutherford, *Langmuir* **2006**, 22, 9967.
[21] S. A. Stern, H. L. Frisch, *Annu. Rev. Mater. Sci.* **1981**, 11, 523.
[22] a) S. He, B. Zhu, X. Jiang, G. Han, S. Li, C. H. Lau, Y. Wu, Y. Zhang, L. Shao, *Proc. Natl. Acad. Sci. USA* **2022**, 119, e2114964119; b) B. Zhu, S. He, Y. Wu, S. Li, L. Shao, *Engineering* **2022**, <https://doi.org/10.1016/j.eng.2022.03.016>.
[23] A. Winter, Y. Ekinci, A. Gözlhäuser, A. Turchanin, *2D Mater.* **2019**, 6, 021002.